Calculation of the EPR g-Tensors of High-Spin Radicals with Density Functional Theory

S. Patchkovskii and T. Ziegler*

Department of Chemistry, University of Calgary, 2500 University Dr. NW, Calgary, Alberta, T2N 1N4 Canada

Received: February 7, 2001; In Final Form: March 27, 2001

The second-order DFT approach of Schreckenbach and Ziegler to the computation of EPR **g** tensors of doublet radicals (*J. Phys. Chem. A* **1997**, *101*, 3388), has been generalized to arbitrary spatially nondegenerate electronic states. The new technique is applied to a large number (47) of diatomic main-group radicals, in $^n\Sigma$ ($n > 2$) ground states. Calculated principal components, of the EPR **g** tensors, are in a good agreement with experiment for main group radicals, with the average errors approaching the accuracy available in experimental matrix isolation studies (VWN average absolute error: 3.8 ppt). The agreement with experiment deteriorates for the mixed, main group−transition metal radicals (VWN error: 8.1 ppt) but the major trends in $\Delta\mathbf{g}_\perp$ values are still reproduced. The approach largely breaks down for radicals containing chemical bonds between two transition metal atoms (VWN error: 30 ppt). In all cases, the calculated **g** tensors are insensitive to the choice of the approximate exchange-correlation functional, with the simple VWN LDA, and gradient-corrected BP86 and RPBE functionals, giving essentially identical results. As an example of the possible future applications of the technique, we examine the **g**-tensor of the first ^3B_u excited state of the trans-$(CNSSS)_2^{2+}$ cation. Our calculations for this systems agree well with the experimental results, both for the magnitudes, and for the orientations of the principal components.

1. Introduction

Electron paramagnetic resonance (EPR), and related techniques, provide an important source of information in experimental studies of systems, containing unpaired electrons.[1,2] EPR spectra are characterized by three principal parameters: EPR **g** tensors describe the interaction of the unpaired electrons with the applied magnetic field. The zero-field splitting (**D**) tensors describe the interactions between the unpaired electrons in the absence of the field. Finally, the hyperfine (**A**) tensors describe the interactions between nuclear and electron magnetic moments. Theoretical techniques for first-principles calculations of hyperfine tensors, and particularly their traces, have been available for some time,[3] and they have proven useful in the interpretation of the experimental data.[4] Although the theory behind the **g** and **D** tensors has been understood early (See,[5] and references therein), accurate first-principles calculations of these quantities, for realistic models, became possible only recently.[6−13] With the development of density functional theory (DFT)[14−16] methods[8,10,12] it is now possible to calculate EPR **g** tensors for radicals with hundreds of atoms. In favorable cases, such calculations can capture the major changes, observed upon chemical or structural modification of the radical,[12,17−20] thus aiding in the interpretation of the experimental results.[21]

Despite this progress, the gamut of radicals, where **g** tensors can be computed with first-principles techniques, is still severely limited by the requirement of spatially nondegenerate, spin-doublet ground state (the Kramers doublet), imposed in most theoretical treatments. Although this restriction is not present in the GUHF[11] and INDO/S[22] approaches, these techniques are either intrinsically incapable of accounting for electron correlation,[11] or rely on empirical adjustable parameters to reproduce the experimental results.[22] As a consequence, EPR **g** tensors of many main-group radicals and metal complexes,[2,4] as well as biological systems of current research interest,[23−26] remain largely inaccessible (but see ref 27) for first-principles calculations.

At the same time, it has been known for some time,[28] that in wave function-based approaches, the theory of EPR **g** tensors allows for a simple generalization to an arbitrary spatially nondegenerate ground state. In this work, we demonstrate that this extension also holds for the DFT formulation of Schreckenbach and Ziegler.[8] We present further the first DFT results for the **g** tensors of a representative selection of spatially nondegenerate high-spin radicals. Section 2 of this work demonstrates the connection between the effective spin-Hamiltonian of EPR spectroscopy and the DFT energy expression. Section 3 summarizes the computational methods, used in this study. Section 4 gives the computational results obtained with the new technique, and compares them to the experimental values. Finally, section 5 presents the conclusions of the present study, and outlines the directions for future developments.

2. Theory

Like other EPR and NMR parameters, the **g** tensor is defined in terms of the phenomenological effective Hamiltonian, chosen to reproduce the experimentally observed spectroscopic transitions. First-principles calculations of the **g** tensor require, that the correspondence between this effective Hamiltonian, and the microscopic Hamiltonian, is established.

The effective spin-Hamiltonian, for a system with the effective spin $\tilde{S} \geq {}^1/_2$, is given by (atomic units)[4]

$$\tilde{H} = g_e \frac{1}{2c}\vec{B}\cdot\hat{\tilde{S}} + p\frac{1}{2c}\vec{B}\cdot\Delta\mathbf{g}\cdot\hat{\tilde{S}} + q\hat{\tilde{S}}\cdot\mathbf{D}\cdot\hat{\tilde{S}} \qquad (1)$$

where g_e is the free-electron g-factor ($g_e \approx 2.0023$[5]), and c is the speed of light ($c \approx 137.04$[29]). Parameters p and q ($p = q =$

10.1021/jp010457a CCC: $20.00 © 2001 American Chemical Society
Published on Web 05/11/2001

1) are used to track orders of the perturbations. Hamiltonian $\tilde{H}$ is defined in the basis of all products of $2\tilde{S}$ α, β one-electron spin functions. The first term in eq 1 represents the Zeeman interaction of the free electron with the magnetic field, whereas the second term describes deviations from the free-electron picture due to the molecular environment. In the high-field limit, the zero-field splitting can be neglected ($q = 0$ in eq 1). Under this assumption, the spin-Hamiltonian can be rewritten as

$$\tilde{H} = \frac{B}{2c}(\alpha_x^2 + \alpha_y^2 + \alpha_z^2)^{1/2}\left\{\frac{\alpha_x\hat{\tilde{S}}_x}{(\alpha_x^2 + \alpha_y^2 + \alpha_z^2)^{1/2}} + \frac{\alpha_y\hat{\tilde{S}}_y}{(\alpha_x^2 + \alpha_y^2 + \alpha_z^2)^{1/2}} + \frac{\alpha_z\hat{\tilde{S}}_z}{(\alpha_x^2 + \alpha_y^2 + \alpha_z^2)^{1/2}}\right\} \quad (2)$$

where the coefficients α_a ($a = x, y, z$) are given by

$$\alpha_a = (\vec{\xi}\cdot\Delta\mathbf{g})_a + g_e\xi_a \quad (3)$$

and $\vec{\xi}$ is a unit vector, in the direction of the magnetic field ($\vec{\xi} = \vec{B}/B$). A unitary transformation of the coordinate system, defined by the Euler angles[30] $\phi = \arctan(\alpha_x/\alpha_y)$ and $\theta = \arctan((\alpha_x^2 + \alpha_y^2)^{1/2}/\alpha_z)$, transforms the operator in the curly braces (eq 2) to a diagonal $\hat{S}'_z$ operator (the choice of the remaining Euler angle, ψ, is arbitrary)

$$\tilde{H} = \frac{B}{2c}(\alpha_x^2 + \alpha_y^2 + \alpha_z^2)^{1/2}\,\hat{S}'_z \quad (4)$$

The eigenvalues of the Hamiltonian (1) in the high-field limit are then given by

$$\tilde{E}_k = k\frac{B}{2c}(g_e{}^2 + 2pg_e(\vec{\xi}\cdot\Delta\mathbf{g}\cdot\vec{\xi}) + p^2\vec{\xi}\cdot(\Delta\mathbf{g}\Delta g^T)\cdot\vec{\xi})^{1/2} \quad (5a)$$

where k varies from $-\tilde{S}$ to $\tilde{S}$, in integer increments. Eigenstates $k = \pm\tilde{S}$ are nondegenerate. All other eigenstates are $\tilde{S}!/(\tilde{S} - k)!k!$-fold degenerate. As long as the deviation from the free electron remains small, eq 5a can be expanded in the first order in p, giving

$$\tilde{E}_k = k\frac{B}{2c}(g_e + p(\vec{\xi}\cdot\Delta\mathbf{g}\cdot\vec{\xi})) + O(p^2) \quad (5b)$$

In the free-electron limit ($p = q = 0$), the two nondegenerate eigenfunctions of the spin-Hamiltonian can be represented by simple products of the α and β spin functions[31]

$$\tilde{\Psi}_{+\tilde{S}}(p = q = 0) = \alpha_1...\alpha_{2\tilde{S}} \quad (6a)$$

$$\Psi_{-\tilde{S}}(p = q = 0) = \beta_1...\beta_{2\tilde{S}} \quad (6b)$$

We can now turn to the examination of the real, microscopic system, described by the effective spin-Hamiltonian. In the Kohn−Sham (KS) formulation of the density functional theory, the KS molecular orbitals (MOs) are obtained by solving a system of effective one-electron eigenequations

$$\hat{f}_\sigma^{KS}\psi_{\sigma i} = \epsilon_{\sigma i}\psi_{\sigma i} \quad (7)$$

where $\sigma = \alpha, \beta$; $i = 1...n_\sigma$ ($n_\alpha \geq n_\beta$); and

$$\hat{f}_\sigma^{KS} = \hat{f}_\sigma^0 + \hat{h}_z + \hat{h}^{10} + \hat{h}^{01} + \hat{h}^{11} \quad (8)$$

Operator $\hat{f}_\sigma^0$ collects all scalar field-free terms. In its simplest form, it is given by

$$\hat{f}_\sigma^0 = -\frac{1}{2}\hat{\Delta} + v_{eff}(\vec{r}) \quad (9)$$

where the effective potential v_{eff} is the sum of the nuclear electrostatic potential, electronic Coulomb potential, and the exchange-correlation potential.[14] Operator $\hat{h}_z$ is the electron Zeeman operator

$$\hat{h}_z = \frac{g_e}{2c}\vec{B}\cdot\hat{s} \quad (10)$$

whereas the operators $\hat{h}^{10}$, $\hat{h}^{01}$, and $\hat{h}^{11}$ collect the remaining terms linear in the magnetic field ($\hat{h}^{10}$), linear in the electron spin ($\hat{h}^{01}$), and bilinear in both ($\hat{h}^{11}$). In their simplest form, these operators are given by[5,8,32]

$$\hat{h}^{10} = -\frac{i}{2c}\vec{B}\cdot(\vec{r}\times\vec{\nabla}) \quad (11)$$

$$\hat{h}^{01} = -\frac{g'i}{4c^2}\hat{s}\cdot\left(\frac{\partial v_{eff}}{\partial\vec{r}}\times\vec{\nabla}\right) \quad (12)$$

$$\hat{h}^{11} = \frac{g'}{8c^3}\left\{\left(\frac{\partial v_{eff}}{\partial\vec{r}}\cdot\vec{r}\right)(\vec{B}\cdot\hat{s}) - (\hat{s}\cdot\vec{r})\left(\frac{\partial v_{eff}}{\partial\vec{r}}\cdot\vec{B}\right)\right\} \quad (13)$$

where $g' = 2g_e - 2$. Operator $\hat{h}^{01}$ is the effective-potential approximation[8] to one- and two-electron spin−orbit coupling operators, given by[5]

$$\hat{h}^{SO} = \frac{g'}{4c^2}\sum_A^{n_{nuc}}\sum_j\hat{s}_j\cdot\left\{\frac{Z_A(\vec{r}_j - \vec{r}_A)\times\hat{p}_j}{|\vec{r}_j - \vec{r}_A|^3}\right\} - \frac{g'}{4c^2}\sum_{j\neq k}\hat{s}_j\cdot\left\{\frac{(\vec{r}_k - \vec{r}_j)\times\hat{p}_j}{|\vec{r}_j - \vec{r}_A|^3}\right\} - \frac{1}{c^2}\sum_{j\neq k}\hat{s}_j\cdot\left\{\frac{(\vec{r}_j - \vec{r}_k)\times\hat{p}_k}{|\vec{r}_j - \vec{r}_k|^3}\right\} \quad (14)$$

where $\hat{p}_j$ is the momentum operator for the electron j, summation over A includes all nuclei in the system, and summation over j and k implicitly includes the electron spin. The effective-potential approximation accounts for the first two contributions to the two-electron spin−orbit operator (the electron−nuclear and electron−electron spin−orbit terms) but neglects the spin-other-orbit (SOO) contribution (the last sum in eq 14). This term is usually quite small, and decreases in importance for heavier radicals.[12,33] Further contributions to eqs 10−13 appear when additional relativistic corrections are considered.[34]

In the second-order approach to the **g** tensors, the scalar field-free Fock operator ($\hat{f}_\sigma^0$) is treated variationally, whereas the remaining operators are applied perturbationally.[8] Once the zeroth-order solutions of the eigenequations 7 are obtained, the resulting Kohn−Sham MOs can be used to construct the Slater determinant, corresponding to the N-electron wave function of the noninteracting KS reference system[14]

$$\Psi_{ref} = ((n_\alpha + n_\beta)!)^{-1/2}\det[\psi_{\alpha1}\alpha, \psi_{\beta1}\beta, ... \psi_{\alpha n_\beta}\alpha, \psi_{\beta n_\beta}\beta, \psi_{\alpha n_\beta+1}\alpha ... \psi_{\alpha n_\alpha}\alpha] \quad (15)$$

The spin part of Ψ_{ref} forms an eigenfunction of the $\hat{S}_z$ operator ($\hat{S}_z = \sum_j\hat{s}_{j,z}$), corresponding to an eigenvalue of $(n_\alpha - n_\beta)/2$. As a consequence, Ψ_{ref} is also an eigenfunction of the total electron Zeeman operator, $(g_e/2c)B\hat{S}_z$. The only remaining requirement,

necessary to establish the relationship between $\tilde{\Psi}_{+\tilde{S}}$ and Ψ_{ref}, is that Ψ_{ref} corresponds to the largest projection of the total spin on the Z axis in this system. This property can be guaranteed by requiring that the spatial MOs $\psi_{\alpha i}$ and $\psi_{\beta i}$ are identical for all i (the spin-restricted approximation).[29] A less severe, but still sufficient constraint, is to require that Ψ_{ref} is an eigenfunction of the $\hat{S}^2$ operator ($\hat{S}^2 = (\sum_j \hat{s}_j)^2$), with an eigenvalue of $(n_\alpha - n_\beta)(n_\alpha - n_\beta + 2)/4$. Although, formally, this property is not guaranteed in spin-unrestricted calculations, the $\hat{S}^2$ expectation values of the DFT reference wave function are often close to this ideal value.[35]

With the correspondence between $\tilde{\Psi}_{+\tilde{S}}$ and Ψ_{ref} established, we require that the derivatives of the microscopic and effective energy levels, with respect to the magnetic field strength, must coincide

$$\frac{\tilde{S}}{2c}(g_e + (\vec{\tilde{\zeta}}\cdot\Delta\mathbf{g}\cdot\vec{\tilde{\zeta}})) = \left.\frac{\partial \tilde{E}_{+\tilde{S}}}{\partial B}\right|_{B=0} = \left.\frac{\partial E^{KS}}{\partial B}\right|_{B=0,s=1/2} = \frac{1}{2}\left.\frac{\partial^2 E^{KS}}{\partial B \partial s}\right|_{B=0,s=0} = \frac{1}{2}\sum_{s,t}\zeta_s\zeta_t \left.\frac{\partial^2 E^{KS}}{\partial B_s \partial s_t}\right|_{B=0,s=0} \quad (16)$$

where E^{KS} is the total energy functional, corresponding to the solutions of the Kohn−Sham eigeneq 7.[14] After examining eq 16 for different orientations of the magnetic field $\vec{\tilde{\zeta}}$, and substituting $(n_\alpha - n_\beta)/2$ for $\tilde{S}$, we obtain

$$\Delta g_{st} = \frac{2c}{(n_\alpha - n_\beta)}\frac{\partial^2 E^{KS}}{\partial B_s \partial s_t} \quad (17)$$

The separation of the off-diagonal Δg_{st} and Δg_{ts} contributions in eq 17 is arbitrary because the eigenvalues of the phenomenological Hamiltonian (eq 5b) can only depend on their sum. Except for the factor $(n_\alpha - n_\beta)^{-1}$, eq 17 is identical to the DFT expression for Δg_{st} of Kramers-type radicals, employed by Schreckenbach and Ziegler.[8] The derivation of the final working expressions for the individual $\Delta\mathbf{g}$ tensor components, starting from the operators 11−13, relies on the spin-field reduction.[29] Because both the derivation and the final equations are completely analogous to the results obtained for the spin-doublet case,[8] they need not be duplicated here.

It should be emphasized that eq 17 is an approximation, which relies on several assumptions. First of all, it is assumed that the (unknown) zeroth-order N-electron wave function of the real interacting system, Ψ_{real}, rather than the noninteracting wave function Ψ_{ref} discussed above, is an eigenfunction of the $\hat{S}^2$ operator. Additionally, our implementation ignores the current dependency of the exchange-correlation functional, neglects the higher-order effects of the spin−orbit coupling operator, and assumes that the SOO contributions in eq 14 are negligible. Given these approximation, the validity of eq 17 should be judged only by its its performance in reproducing the experimental **g** values of high-spin radicals.

In passing, we note that is was recently suggested[12] that the *exact* results for the spin−orbit coupling operator in the real, interacting system, can be obtained by evaluating the matrix elements of the two-electron operator 14, between the noninteracting reference wave function (eq 15) and the corresponding singly excited Slater determinants. Obviously, this can only be true if the noninteracting wave function Ψ_{ref} is identical to the (unknown) interacting N-electron wave function Ψ_{real}. As a consequence, the approach of ref 12 to the spin−orbit matrix elements, in fact, constitutes an approximation. The consequences of this approximation can be examined from the well-understood[14,36] properties of the exchange-correlation (XC) holes in the noninteracting reference and in the real, interacting system. By definition, the XC hole of the reference system does not contain any correlation contributions. In the interacting system, the correlation contribution reduces the probability of the close contact between the electrons but increases it at larger separations.[36] From the form of the two-electron part of the SO coupling operator (second sum in eq 14), which is dominated by close inter-electronic contacts, neglect of the correlation contribution to the XC hole should lead to excessively large two-electron contributions. The approximation 12, which incorporates the complete exchange-correlation potential into v_{eff}, properly accounts for the shape of the complete XC hole of the real, interacting system and does not suffer from this problem. At the same time, the direct application of eq 14 to the KS reference wave function allows incorporation of the spin-other-orbit contributions. On the balance, the approximation of ref 12 is likely to lead to superior results for systems, where correlation gives a negligible contribution to the shape of the XC hole, whereas the SOO terms are significant. At the same time, the effective potential approximation (eq 12) should be superior for systems exhibiting strong correlation effects.

3. Methods

All calculations are based on DFT,[14−16] and were performed with the Amsterdam density functional (ADF) program package,[37−39] using Cartesian space numerical integration[40] and analytical gradients for the geometry optimization.[32,41] The implementation of the EPR **g** tensors, due to Schreckenbach and Ziegler,[8] was extended to allow treatment of high-spin radicals, as discussed above. An uncontracted, triple-ζ basis of Slater-type orbitals was employed for the $(n-1)$f (if present), ns, np, nd, $(n+1)$s, and $(n+1)$p valence shells of the transition metal elements and the $(n-1)$d (if present), ns, and np shells of the main group elements. The basis set was augmented by a set of polarization functions for main-group elements, and is designated as the standard basis set IV[42] in ADF. Inner shells were treated within the frozen core approximation.[38] To test convergence of the results, with respect to the basis set size, EPR **g** tensor in one system (V_2^+) was also computed using an extended basis set of triple-ζ, double polarization quality. In this case, the standard basis IV was augmented with two 4d basis functions ($\zeta = 1.70, 1.08$) and two 4f basis functions ($\zeta = 5.20, 2.43$). The single 4p polarization function of the standard basis set was replaced with two 4p functions ($\zeta = 1.58, 0.95$). The extended basis set is designated as IV′. In all calculations, scalar relativistic effects were included within the quasi-relativistic framework[43] employing relativistic frozen core potentials, in conjunction with the first-order Pauli Hamiltonian. Molecular geometries were fully optimized using BP86[44,45] generalized gradient approximation (GGA) functional. Optimized molecular geometries are included in the Supporting Information. EPR **g** tensors were computed using VWN[46] local density approximation (LDA) functional as described elsewhere.[8,34] For comparison, the **g** tensors were also evaluated with BP86[44,45] and RPBE[47−49] gradient-corrected functionals. The latter functional was recently demonstrated to provide a significant improvement,[50] over both LDA and "classical" GGAs, in calculation of atomization energies. All calculations, both in geometry optimization and in the evaluation of the **g** tensors, employed spin-unrestricted wave functions. In all cases, the experimental spin multiplicities were used in the calculations. A special care was taken to ensure that, for linear molecules, SCF solutions converge to axially symmetric charge distribu-

tions, expected from the spatially nondegenerate $^n\Sigma$ electronic ground states in these radicals.

4. Results and Discussion

To examine the performance of the new approach, we compared the experimental and calculated EPR **g** tensors for selected diatomic high-spin radicals. A large body of reliable experimental data for such radicals, covering a substantial fraction of the periodic table, is available.[4] These experimental values were obtained in inert gas matrices, or in gas phase, which should reduce the environmental influences. Typically, **g** tensors measured in inert matrices agree with gas-phase results to within a few ppt, with larger deviations observed for heavy and easily polarizable molecules[4] (Also see refs 51−54). Most of the gas-phase $\Delta\mathbf{g}_\perp$ values were computed from the experimental spin-rotational parameters, with the use of the Curl's equation.[55,56] The $\Delta\mathbf{g}_\perp$ values, computed from the Curl's relation, are usually in a good agreement with the results of the direct experimental measurements of the **g** tensor components.[4] Because the present technique is limited to spatially nondegenerate electronic states, only radicals in $^n\Sigma$ ($n > 2$) ground states were included in this study.

In linear molecules, only two distinct principal components of the **g** tensor are allowed by symmetry. The principal component, oriented along the molecular axis, is designated as $\mathbf{g}_\parallel$. The doubly degenerate component, in a direction perpendicular to the molecular axis, is $\mathbf{g}_\perp$. Instead of the **g** values, it is convenient to work with the deviations from the free-electron values g_e, defined as

$$\Delta\mathbf{g}_\parallel = \mathbf{g}_\parallel - g_e \tag{18a}$$

$$\Delta\mathbf{g}_\perp = \mathbf{g}_\perp - g_e \tag{19b}$$

For the radicals considered in this study, magnitudes of the $\Delta\mathbf{g}$ values vary from ca. 10^{-3} to 0.1, and can, therefore, be conveniently expressed in parts per thousand (ppt).

In homonuclear $^n\Sigma$ diatomics, the paramagnetic contribution to the $\Delta\mathbf{g}_\parallel$, which usually dominates deviations from the free-electron value, vanishes by symmetry.[4] Although not exactly zero, this contribution is typically quite small in heteronuclear diatomics as well. As a consequence, $\Delta\mathbf{g}_\parallel$ values for all diatomic radicals, included in this study, are dominated by the (small) relativistic mass−velocity correction. All calculated $\Delta\mathbf{g}_\parallel$ values are in the range of −0.3 to 0.0 ppt. Where available, the experimental $\Delta\mathbf{g}_\parallel$ values are also rather small. In fact, the analysis of the experimental EPR spectra, for $^n\Sigma$ radicals, frequently assumes that the value is negligible.[4] Therefore, we will not show any results for $\Delta\mathbf{g}_\parallel$, and will not discuss these values any further.

Calculated VWN, BP86, and RPBE $\Delta\mathbf{g}_\perp$ values, for 47 $^n\Sigma$ radicals, are collected in Table 1, in comparison with the available experimental data. The statistical evaluation of the results is given in Table 2. The results clearly separate into three distinct categories, depending on the nature of the radical. For main group radicals, calculated $\Delta\mathbf{g}_\perp$ values are, generally, in a good agreement with experiment, as can be seen from the correlation diagram (Figure 1). For more than half of the radicals (10 out of 19), calculated and experimental values agree to within 1 ppt. The average absolute error, for this class of radicals, is 3.8 ppt (VWN). Notably, gradient-corrected functionals so not improve significantly upon the LDA results, with the average errors of 3.4 (BP86) and 3.5 ppt (RPBE). The individual $\Delta\mathbf{g}_\perp$ values, calculated with all three functionals, are also essentially identical (Table 1).

TABLE 1: Calculated VWN, BP86, and RPBE $\Delta\mathbf{g}_\perp$ Values (in ppt), for High-Spin $^n\Sigma$ ($n > 2$) Diatomic Radicals, in Comparison with Experimental Results

molecule	n[a]	VWN	BP86	RPBE	expt	reference
B_2	3	0.3	0.2	0.2	−0.8	61
O_2	3	3.3	3.1	3.1	2.9[b]	62
SO	3	4.8	4.6	4.6	3.6[b]	63
SeO	3	18.2	17.9	17.6	32.7[b,c]	57
S_2	3	12.6	12.1	11.9	14.5[b]	4
NH	3	1.9	1.5	1.5	1.7[b]	4
NF	3	2.2	2.0	2.0	2.0[b]	64
NCl	3	5.6	5.0	4.9	5.4[b]	65
NBr	3	24.2	21.8	21.3	19.3[b]	66
NI	3	43.6	38.9	38.2	31.0[b]	67
PH	3	4.8	4.1	4.0	4.5[b]	4
BC	4	0.1	−0.1	−0.1	−0.3	68
C_2^+	4	−0.6	−0.6	−0.6	−0.5	69
AlC	4	−1.4	−1.4	−1.3	−1.3	70
Si_2^+	4	−6.0	−5.9	−5.8	−9.3	52
Ge_2^+	4	−50.4	−49.2	−47.7	−63.3	52
SiB	4	−1.1	−1.2	−1.1	−1.8	71
SiAl	4	−3.8	−3.7	−3.6	−4.5	71
$GaAs^+$	4	−21.9	−20.3	−19.0	−4.5	72
VO	4	−21.4	−18.1	−15.8	−21.9	73
CrN	4	−5.3	−5.0	−3.2	−5.6[b]	74
MoN	4	−4.6	−4.2	−4.6	−10.9[b,d]	74
YB^+	4	−35.3	−28.1	−29.9	−42.3	75
YAl^+	4	−72.1	−52.9	−47.1	−60.3	75
NbO	4	−30.7	−27.7	−25.9	−44.6	76
CrH	6	−4.4	−4.6	−7.6	2.7	4
CrF	6	−12.8	−11.0	−10.7	−1.3	4
MnO	6	2.5	2.5	2.0	−7.3	4
MnS	6	11.4	10.2	10.0	6.7	4
MnH	7	−2.0	−2.0	−2.4	−1.3	4
MnF	7	0.3	0.1	−0.3	−1.3	4
MnCl	7	1.3	0.9	0.3	−7.3	4
MnBr	7	6.1	5.1	3.3	−9.3	4
MnI	7	12.5	10.7	8.8	−9.3	4
V_2^+	4	−11.4	−11.3	−10.9	−46.3	54
TiV	4	−14.3	−15.1	−15.1	−24.3	77
TiNb	4	−21.3	−26.7	−27.5	−73.8	77
ZrV	4	−20.7	−21.7	−22.3	−41.3	77
ZrNb	4	−34.7	−37.5	−37.5	−98.8	77
HfV	4	−57.8	−55.8	−55.0	−93.8	77
CrAg	6	−1.0	−1.3	−1.3	1.7[e]	78
WCu	6	−67.7	−58.4	−51.1	−106.3	78
WAg	6	−78.5	−65.2	−59.8	−106.3	78
WAu	6	−35.9	−29.4	−24.9	−92.3	78
CrAu	6	29.6	25.0	24.1	−1.3	78
MnAg	7	4.2	3.5	3.3	−4.3	4
Mn_2^+	12	2.4	2.0	8.9	−3.3	79

[a] Term multiplicity. [b] Estimated from gas-phase rotational parameters, using Curl's relation.[55,56] [c] Estimated error bar ±11 ppt. [d] An alternative experimental value of −33 ppt, measured in Ne matrix, was also reported.[80] [e] An alternative experimental value of −52 ± 3 ppt, measured in Ar matrix, was also reported.[4]

The worst outliers on the main group $\Delta\mathbf{g}_\perp$ correlation plot are SeO (VWN: +18, expt: +33 ppt), Ge_2^+ (VWN: −50, expt: −63 ppt) and isoelectronic $GaAs^+$ (VWN: −22, expt: −5 ppt), and NI (VWN: +44, expt: +31 ppt). For the $^3\Sigma$ selenium oxide, the experimental error is estimated at ≈11 ppt, or $^1/_3$ of the experimental value.[57] Taking a value at the lower side of the experimental error bar (+22 ppt), would lead to a much better agreement with the calculated result. For the Ge_2^+ cation, the situation is more interesting. The Ge−Ge chemical bond in this radical is quite weak, despite the formal 1.5 bond order (Figure 2, upper panel), whereas the calculated $\Delta\mathbf{g}_\perp$ component exhibits a strong dependence on the interatomic distance (the lower panel). The optimized BP86 geometry, used in our

TABLE 2: Statistical Evaluation of the Performance of VWN, BP86, and RPBE Exchange-Correlation Functionals, in Calculation of the $\Delta g_\perp$ Values of High-Spin Diatomic Radicals

	all	MG−MG[a]	TM−MG[a]	TM−TM[a]
data points	47	19	15	13
range, ppt	138	95	67	108
VWN				
ave.[b]	9.6	0.3	3.9	29.5
abs.[c]	12.4	3.8	8.1	29.9
RMS[d]	20.0	6.7	10.1	35.6
BP86				
ave.[b]	10.4	0.0	6.0	30.7
abs.[c]	12.7	3.4	8.3	31.1
RMS[f]	20.7	6.2	10.1	37.1
RPBE				
ave.[b]	10.9	0.0	6.0	32.4
abs.[c]	13.3	3.5	8.8	32.9
RMS[d]	21.7	6.3	10.3	39.0

[a] MG = main group atom; TM = transition metal atom. [b] Average signed error, in ppt. [c] Average absolute error, in ppt. [d] Root-mean-square error, in ppt.

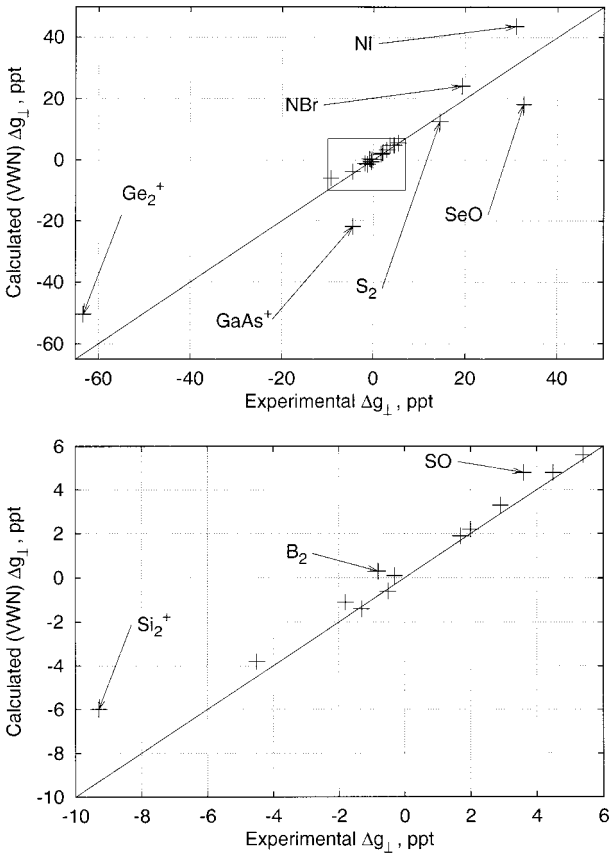

Figure 1. Correlation between calculated (VWN) and experimental $\Delta g_\perp$ values, for main group diatomic radicals. Diagonal line represents the perfect agreement between theory and the experiment. The lower panel gives the expanded view of the central part of the correlation diagram. The radicals, for which deviations from the experiment exceed 1 ppt, are indicated by the arrows.

g-tensor calculations, was obtained in the gas phase. At the same time, the experimental EPR measurement was performed in solid Ne matrixes,[52] where bond lengths may be influenced by environmental effects. Elongation of the Ge−Ge bond, from the optimized gas-phase value of 2.46 Å, to approximately 2.7 Å, would bring the calculated $\Delta g_\perp$ value (−59 ppt) into a good agreement with experiment (−63 ppt). According to BP86 calculations, such elongation would require only 3.5 kcal/mol

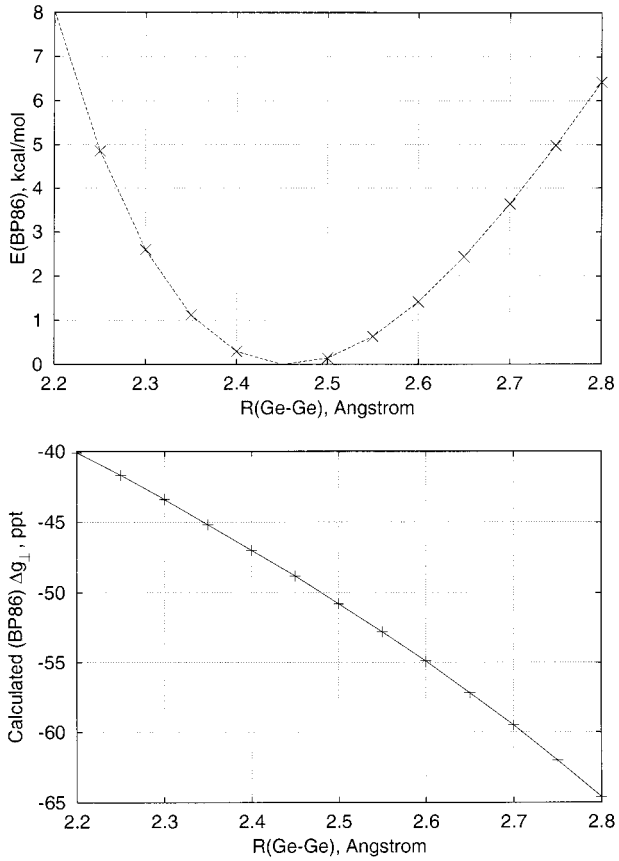

Figure 2. Calculated (BP86) potential energy (upper panel) and $\Delta g_\perp$ values (lower panel), for the lowest $^4\Sigma$ state of Ge_2^+, as functions of the interatomic distance.

in the gas phase. Additionally, BP86 calculations indicate the presence of an electronically excited $^2\Sigma$ state within 0.5 eV of the $^4\Sigma$ ground state of Ge_2^+. Contributions, due to these states, can influence the calculated **g** tensors through second-order spin−orbit coupling effects, neglected in our calculations. Such effects are known to be important for the accurate description of properties in some of the high-spin diatomic radicals.[58]

Higher-order contributions are likely to be responsible for the large error found for NI as well. In this respect, it is instructive to examine the isovalent series of $^3\Sigma$ radicals, consisting of NH, NF, NCl, NBr, and NI (Table 1). For the first three members of the series, calculated $\Delta g_\perp$ values agree with experiment, to within the accuracy expected from the Curl's[4,55] relation. At the same time, the calculated $\Delta g_\perp$ values for NBr are noticeably too large (VWN: 24 ppt, expt: 19 ppt). For the heaviest member of the series, NI, the calculated $\Delta g_\perp$ values are clearly too positive, by about a third (VWN: 44 ppt, expt: 31 ppt). The importance of the second-order spin−orbit coupling effects is expected to increase in the same series.

The quality of the theoretical results deteriorates noticeably for the mixed, main group−transition metal radicals. The average absolute deviation (VWN: 8.1 ppt) from experiment, for such radicals, increases by more than a factor of 2, compared to the main group systems (VWN: 3.8 ppt). All three functionals examined perform equally well (see Table 2). With one exception, the calculated $\Delta g_\perp$ values still show a reasonable correlation with the experimental results (Figure 3). Nonetheless, some qualitative failures become also apparent. Thus, the experimental $\Delta g_\perp$ values *decrease* in the MnX series MnH ≈ MnF > MnCl > MnBr ≈ MnI. On the other hand, the calculated $\Delta g_\perp$ values actually *increase* in the same series, with the largest

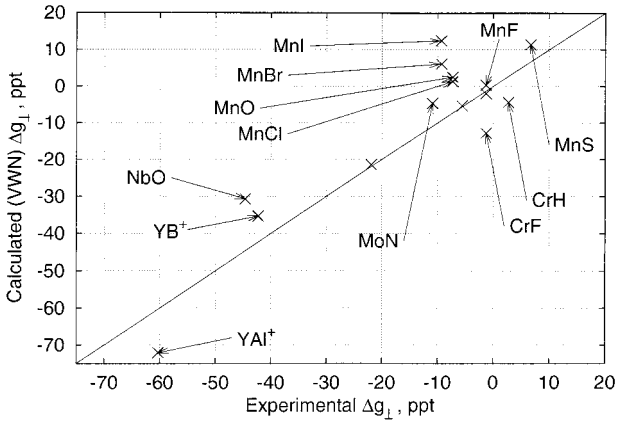

Figure 3. Correlation between calculated (VWN) and experimental $\Delta\mathbf{g}_\perp$ values, for the mixed transition metal−main group radicals. Diagonal line represents the perfect agreement between theory and the experiment. The radicals, for which deviations from experiment exceed 1 ppt, are indicated by the arrows.

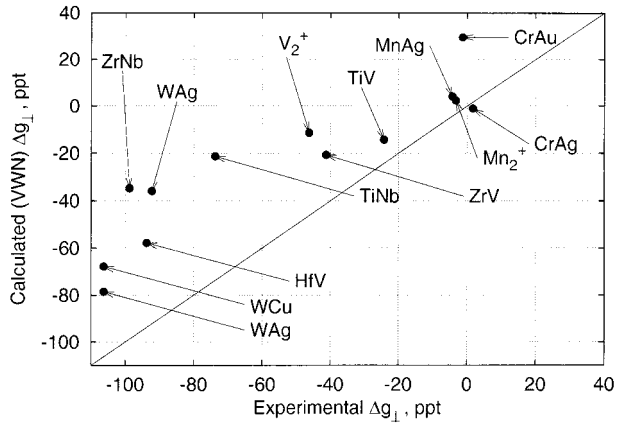

Figure 4. Correlation between calculated (VWN) and experimental $\Delta\mathbf{g}_\perp$ values, for the transition metal diatomic radicals. Diagonal line represents perfect agreement between theory and experiment. The radicals, for which deviations from the experiment exceed 1 ppt, are indicated by the arrows.

deviations from the experiment found for the heavier halogens X (Br and I). A combination of the higher-order SO coupling effects, and the increased importance of the environment for larger halogen atoms, is likely responsible for this failure. In previous studies of doublet metal radicals,[12,18,19] deviations from the experiment were also found to increase for heavier metal centers. Unfortunately, our present data set is not sufficiently large to verify whether this observation applies to high-spin radicals.

Finally, the correlation between the experimental and calculated $\Delta\mathbf{g}_\perp$ values largely breaks down for the transition metal diatomic radicals (Figure 4). Although the calculations seem to follow the gross trends in $\Delta\mathbf{g}_\perp$, calculated values are systematically too positive, with deviations increasing for larger $\Delta\mathbf{g}_\perp$ magnitudes. Again, the choice of the density functional does not appear to be important, with both VWN LDA and GGAs, leading to similar, poor results. The average absolute errors for all three functionals are 30 ppt or more, compared to the total experimental range of 108 ppt. Calculated $\Delta\mathbf{g}_\perp$ values, in transition metal diatomics, appear to be reasonably converged with respect to the basis set size. Thus, BP86 calculations on V_2^+, using the extended IV′ basis set, give $\Delta\mathbf{g}_\perp = -11.0$ ppt, compared to -11.3 ppt for the smaller basis IV.

Although disappointing, this failure is not entirely unexpected. Transition metal diatomics are known to possess a multitude of close-lying electronically excited states, and therefore, present a severe challenge to both approximate DFT and ab initio techniques.[35,59] The difficulties, encountered in calculations, aiming at the prediction of molecular structures and atomization energies are exacerbated in EPR **g**-tensor calculations, due to their sensitivity to the energies and shapes of the Kohn−Sham MOs, in the vicinity of the singly occupied MOs.

TABLE 3: Comparison of the Calculated and Experimental[60] $\Delta\mathbf{g}_\perp$ Tensors for $(CNSSS)_2^{2+}$

	VWN	BP86	RBPE	expt
$\Delta\mathbf{g}_1$[a], ppt	−0.7	−0.7	−0.6	-0.1 ± 0.1
$\Delta\mathbf{g}_2$[b], ppt	+13.2	+13.1	+13.1	$+14.8 \pm 0.2$
$\Delta\mathbf{g}_3$[b], ppt	+21.6	+21.2	+21.2	$+24.8 \pm 0.2$
γ_3[c], degree	+20.6	+20.4	+20.5	$+16 \pm 2$

[a] Component in the direction perpendicular to the molecular σ_h plane of symmetry. [b] Component within the σ_h plane. [c] Angle between the $\Delta\mathbf{g}_3$ component, and the direction of the C−C bond. Positive no.s indicate displacements toward the C−S bond, and away from the C−N bond of the cation. All other orientational parameters are fixed by symmetry.

Overall, our results suggest that density functional theory calculations can predict EPR **g**-tensors of light, main-group radicals with the accuracy comparable to a routine experimental measurement. It can also provide an indication of trends and approximate magnitudes of **g** tensor components, for radicals containing heavier nuclei, including transition metals, provided that no metal−metal bonds are involved.

To further illustrate the practical utility of DFT calculations, in the analysis of the **g**-tensors of high-spin radicals, we consider a somewhat more involved case, *trans*-$(CNSSS)_2^{2+}$. This system provides a rare example of a thermally accessible excited triplet state (of the ^3B_u symmetry), for which a meticulous experimental measurement of the complete EPR **g**- and **D**-tensors is available.[60] Calculated VWN, BP86, and RPBE $\Delta\mathbf{g}$ tensor components, and their orientations, relative to the local coordinate system of $(CNSSS)_2^{2+}$, are given in Table 3, in comparison with the experimental results. As already seen for the diatomic radicals, the choice of the density functional influences the results only marginally. Calculated magnitudes of the principal components are in a good agreement with experiment (VWN: $\Delta\mathbf{g}_1 = -0.7$, $\Delta\mathbf{g}_2 = +13.2$, $\Delta\mathbf{g}_3 = +21.6$ ppt; expt: $\Delta\mathbf{g}_1 = -0.1 \pm 0.1$, $\mathbf{g}_2 = +14.8 \pm 0.2$, $\mathbf{g}_3 = +24.8 \pm 0.2$). Because of the high symmetry of the cation, only one orientational parameter, the angle between the C═C bond direction and the orientation of the largest principal component ($\mathbf{g}_3$), is not determined a priori. For this parameter, the calculated value (VWN: 21°) agrees well with the experimental result (16 ± 2°).

5. Conclusions and Outlook

We have shown, that the second-order DFT approach to the EPR **g**-tensors, originally developed by Schreckenbach and Ziegler for doublet Kramers-type radicals,[8] can be generalized easily, allowing treatment of arbitrary radicals in spatially nondegenerate electronic states. The new technique is applied to a large number (47) of diatomic main-group radicals, in $^n\Sigma$ ($n > 2$) ground states. Calculated principal components of the EPR **g** tensors are in a good agreement with experiment for main group radicals, with the average errors approaching the accuracy available in experimental matrix isolation studies (VWN average absolute error: 3.8 ppt). Deviations from experiment tend to increase for heavier elements, with the best results obtained for radicals from the first three rows of the periodic table.

The agreement with experiment deteriorates somewhat for the mixed, main group − transition metal radicals (VWN error: 8.1 ppt), but the major trends in $\Delta\mathbf{g}_\perp$ values are still reproduced. The approach largely breaks down for radicals, containing chemical bonds between two transition metal atoms (VWN error: 30 ppt). In all cases, the calculated **g** tensors are insensitive to the choice of the approximate exchange-correlation functional, with simple VWN LDA, and gradient-corrected BP86 and RPBE functionals, leading to essentially identical results.

At least in some cases, the failure of the calculations can be attributed to the neglect of the higher-order effects of the spin−orbit coupling operator. Incorporation of these contributions may be expected to improve agreement with the experiment for the heavier radicals, such as NI ($^3\Sigma$). Calculated **g** tensor components show a strong dependence on the bond lengths. As a consequence, environmental and thermal effects may play a substantial role, particularly in weakly bound radicals, such as Ge_2^+ ($^4\Sigma$).

The future extensions of this work may include incorporation of second-order spin−orbit coupling effects and a generalization to spatially degenerate ground states. Even without such enhancements, the present extension of the DFT techniques to **g**-tensors of non Kramers-type systems exposes for the first time a large number of experimentally interesting radicals, to a detailed theoretical scrutiny. As an example of the possible applications of the technique, we examine the **g**-tensor of the first ^3B_u excited state of *trans*-$(CNSSS)_2^{2+}$ cation. Our calculations for this systems agree with the experimental results to a good accuracy, both for the magnitudes, and for the orientations of the principal components.

Acknowledgment. This work has been supported by the National Sciences and Engineering Research Council of Canada (NSERC), as well as by the donors of the Petroleum Research Fund, administered by the American Chemical Society. We acknowledge Dr. Stan van Gisbergen for pointing out a small discrepancy between our implementation of the RPBE functional and the reference code.

Supporting Information Available: Optimized BP86 bond length of the 47 high-spin diatomic radicals and the optimized geometry of the *trans*-$(CNSSS)_2^{2+}$ cation (1 page). This material is available free of charge via the Internet at http://pubs.acs.org.

References and Notes

(1) Wertz, J. E.; Bolton, J. R. *Electron Spin Resonance*; Chapman and Hall: New York, 1986.
(2) Abragam, A.; Bleaney, B. *Electron Paramagnetic Resonance of Transition Ions*; Clarendon: Oxford, 1970.
(3) Pople, J. A.; Beveridge, D. L.; Dobosh, P. A. *J. Am. Chem. Soc.* **1968**, *90*, 4101.
(4) Weltner, W., Jr. *Magnetic Atoms and Molecules* Dover, New York, 1983.
(5) Harriman, J. E. *Theoretical Foundations of Electron Spin Resonance*; Academic Press: New York; 1978.
(6) Lushington, G. H.; Bündgen, P.; Grein, F. *Int. J. Quantum Chem.* **1995**, *55*, 377.
(7) Lushington, G. H.; Grein, F. *Int. J. Quantum Chem.* **1996**, *60*, 1679.
(8) Schreckenbach, G.; Ziegler, T. *J. Phys. Chem. A* **1997**, *101*, 3388.
(9) Vahtras, O.; Minaev, B.; Ågren, H. *Chem. Phys. Lett.* **1997**, *281*, 186.
(10) van Lenthe, E.; Wormer, P. E. S.; van der Avoird, A. *J. Chem. Phys.* **1997**, *107*, 2488.
(11) Jayatilaka, D. *J. Chem. Phys.* **1998**, *108*, 7587.
(12) Malkina, O. L.; Vaara, J.; Schimmelpfenning, B.; Munzarová, M.; Malkin, V. G.; Kaupp, M. *J. Am. Chem. Soc.* **2000**, *122*, 9206.
(13) Lushington, G. H. *J. Phys. Chem. A* **2000**, *104*, 2969.
(14) Parr, R. G.; Yang, W. *Density Functional Theory of Atoms and Molecules*; Oxford University: Oxford, 1989.
(15) Ziegler, T. *Chem. Rev.* **1991**, *91*, 651.
(16) Salahub, D. R.; Castro, M.; Proynov, E. Y. *Relativistic and Electron Correlation Effects in Molecules and Solids;* Malli, G. L., Ed.; Plenum: New York, 1994.
(17) Schreckenbach, G.; Ziegler, T. *Theor. Chem. Acc.* **1998**, *99*, 71.
(18) Patchkovskii, S.; Ziegler, T. *J. Chem. Phys.* **1999**, *111*, 5730.
(19) Patchkovskii, S.; Ziegler, T. *J. Am. Chem. Soc.* **2000**, 122, 3506.
(20) van Lenthe, E.; van der Avoird, A.; Hagen, W. R.; Reijerse, E. J. *J. Phys. Chem. A.* **2000**, *104*, 2070.
(21) Patchkovskii, S.; Ziegler, T. *Inorg. Chem.* **2000**, *39*, 5354.
(22) Neese, F.; Solomon, E. I. *Inorg. Chem.* **1998**, *37*, 6568.
(23) Campbell, K. A.; Yikilmaz, E.; Grant, C. V.; Gregor, W.; Miller, A.-F.; Britt, R. D. *J. Am. Chem. Soc.* **1999**, *121*, 4714.
(24) Campbell, K. A.; Force, D. A.; Nixon, P. J.; Dole, F.; Diner, B. A.; Britt, R. D. *J. Am. Chem. Soc.* **2000**, *122*, 3754.
(25) Käss, H.; MacMillan, F.; Ludwig, B.; Prisner, T. F. *J. Phys. Chem. B* **2000**, *104*, 5362.
(26) Krebs, C.; Davydov, R.; Baldwin, J.; Hoffman, B. M.; Bollinger, J. M., Jr.; Huynh, B. H. *J. Am. Chem. Soc.* **2000**, *122*, 5327.
(27) Case, D. A. *J. Chem. Phys.* **1985**, *83*, 5792.
(28) Stone, A. J. *Proc. R. Soc. (London) A* **1963**, *271*, 424.
(29) McWeeny, R. *Methods of Molecular Quantum Mechanics*, 2nd ed.; Academic: London, 1992.
(30) Poole, C. P., Jr. *The Physics Handbook*; Wiley: New York, 1998.
(31) Poole, C. P., Jr.; Forsch, H. A. *The Theory of Magnetic Resonance*; Wiley: New York, 1972.
(32) Schreckenbach, G.; Ziegler, T. *J. Phys. Chem.* **1995**, *99*, 606.
(33) Malkina, O. L.; Schimmelpfenning, B.; Kaupp, M.; Hess, B. A.; Chandra, P.; Wahlgren, U.; Malkin, V. G. *Chem. Phys. Lett.* **1998**, *296*, 93.
(34) Schreckenbach, G. *Relativity and Magnetic Properties. A Density Functional Study*, Ph.D. Thesis, University of Calgary: Calgary, 1996.
(35) Barden, J. B.; Rienstra-Kiracofe, J. C.; Schaefer, H. F., III *J. Chem. Phys.* **2000**, *113*, 690.
(36) Baerends, E. J.; Gritsenko, O. V. *J. Phys. Chem. A* **1997**, *101*, 5383.
(37) ADF 2.3.3, http://tc.chem.vu.nl/SCM.; Department of Theoretical Chemistry, Vrije Universiteit: Amsterdam.
(38) Baerends, E. J.; Ellis, D. E.; Ros, P. *Chem. Phys.* **1973**, *2*, 41.
(39) Fonseca Guerra, C.; Visser, O.; Snijders, J. G.; te Velde, G.; Baerends, E. J. *Methods and Techniques in Computational Chemistry METECC-95*; Clementi, E., Corongiu, G., Eds.; STEF: Cagliari, 1995; pp 305−395.
(40) te Velde, G.; Baerends, E. J. *J. Comput. Chem.* **1992**, *9*, 84.
(41) Versluis, L.; Ziegler, T. *J. Chem. Phys.* **1988**, *88*, 322.
(42) All standard ADF basis sets are available on the Internet at: "http://www.scm.com/Doc/atomicdata/".
(43) Ziegler, T.; Tschinke, V.; Baerends, E. J.; Snijders, J. G.; Ravenek, W. *J. Phys. Chem.* **1989**, *93*, 3050.
(44) Becke, A. D. *Phys. Rev. A* **1988**, *38*, 3098.
(45) Perdew, J. P. *Phys. Rev. B* **1986**, *33*, 8822; **1986**, *34*, 7406.
(46) Vosko, S. H.; Wilk, L.; Nusair, M. *Can. J. Phys.* **1980**, *58*, 1200.
(47) Perdew, J. P.; Burke, K.; Ernzerhof, M. *Phys. Rev. Lett.* **1996**, *77*, 3865.
(48) Hammer, B.; Hansen, L. B.; Norskov, J. K. *Phys. Rev. B* **1999**, *59*, 7413.
(49) Patchkovskii, S. *Self-Consistent Implementation of Perdew-Burke-Ernzerhof and related GGAs in ADF. Technical Report*, Calgary, 2000.
(50) Matveev, A.; Staufer, M.; Mayer, M.; Rösch, N. *Int. J. Quantum Chem.* **1999**, *75*, 863.
(51) Hamrick, Y. M.; Weltner, W., Jr. *J. Chem. Phys.* **1991**, *94*, 3371.
(52) Knight, L. B., Jr.; Herlong, J. O.; Babb, R.; Earl, E.; Hill, D. W.; Arrington, C. A. *J. Phys. Chem.* **1991**, *95*, 2732.
(53) Van Zee, R. J.; Li, S.; Weltner, W., Jr. *Chem Phys. Lett.* **1994**, *217*, 381.
(54) Knight, L. B., Jr.; Babb, R.; Ray, M.; Banisaukas, T. J., III *J. Chem. Phys.* **1996**, *105*, 10 237.
(55) Curl, R. F. *Mol Phys.* **1965**, *9*, 585.
(56) Knight, L. B., Jr.; Weltner, W., Jr. *J. Chem. Phys.* **1970**, *53*, 4111.
(57) Carrington, A.; Currie, G. N.; Levy, D. H.; Miller, T. A. *Mol. Phys.* **1969**, *17*, 535.
(58) Kayama, K.; Baird, J. C. *J. Chem. Phys.* **1967**, *46*, 2604.
(59) Desmarais, N.; Reuse, F. A.; Khanna, S. N. *J. Chem. Phys.* **2000**, *112*, 5576.
(60) Berces, A.; Enright, G. D.; McLaurin, G. E.; Morton, J. R.; Preston, K. F.; Passmore, J.; Wood, D. *J. Magn. Res. Chem.* **1999**, *37*, 353.
(61) Knight, L. B., Jr.; Gregory, B. W.; Cobranchi, S. T.; Feller, D.; Davidson, E. R. *J. Am. Chem. Soc.* **1987**, *109*, 3521.
(62) Tinkham, M.; Strandberg, M. W. P. *Phys. Rev.* **1955**, *97*, 951.
(63) Uehara, H. *Bull. Chem. Soc. Jpn.* **1969**, *42*, 886.
(64) Douglas, A. E.; Jones, W. E. *Can. J. Phys.* **1966**, *44*, 2251.
(65) Yamada, C.; Endo, Y.; Hirota, E. *J. Chem. Phys.* **1983**, *79*, 4159.

(66) Sakamaki, T.; Okabayashi, T.; Tanimoto, M. *J. Chem. Phys.* **1998**, *109*, 7169.
(67) Sakamaki, T.; Okabayashi, T.; Tanimoto, M. *J. Chem. Phys.* **1999**, *111*, 6345.
(68) Knight, L. B., Jr.; Cobranchi, S. T.; Petty, J. T.; Earl, E.; Feller, D.; Davidson, E. R. *J. Chem. Phys.* **1989**, *90*, 690.
(69) Knight, L. B., Jr.; Cobranchi, S. T.; Earl, E. *J. Chem. Phys.* **1988**, *88*, 7348.
(70) Knight, L. B., Jr.; Cobranchi, S. T.; Herlong, J. O.; Arrington, C. A. *J. Chem. Phys.* **1990**, *92*, 5856.
(71) Knight, L. B., Jr.; McKinkey, A. J.; Babb, R. M.; Morse, M. D.; Arrington, C. A. *J. Chem. Phys.* **1993**, *98*, 6749.
(72) Knight, L. B., Jr.; Petty, J. T. *J. Chem. Phys.* **1988**, *88*, 481.
(73) Kasai, P. H. *J. Chem. Phys.* **1968**, *49*, 4979.
(74) Namiki, K.-i. C.; Steimie, T. C. *J. Chem. Phys.* **1999**, *111*, 6385.
(75) Knight, L. B., Jr.; Babb, R. M.; King, G. M.; McKinley, A. J. *J. Chem. Phys.* **1993**, *98*, 4404.
(76) Brom, J. M., Jr.; Durham, C. H., Jr.; Weltner, W., Jr. *J. Chem. Phys.* **1974**, *61*, 970.
(77) Van Zee, R. J.; Weltner, W., Jr. *J. Chem. Phys.* **1995**, *103*, 2762.
(78) Hamrick, Y. M.; Van Zee, R. J.; Weltner, W., Jr. *Chem. Phys. Lett.* **1991**, *181*, 193.
(79) Cheeseman, M.; Van Zee, R. J.; Flanagan, H. L.; Weltner, W., Jr. *J. Chem. Phys.* **1990**, *92*, 1553.
(80) Knight, L. B., Jr.; Steadman, J. *J. Chem. Phys.* **1982**, *76*, 3378.